Chemistry & Biology, Vol. 9, 679–690, June, 2002, ©2002 Elsevier Science Ltd. All rights reserved. PII S1074-5521(02)00163-1

Path of an RNA Ligand around the Surface of the Vaccinia VP39 Subunit of Its Cognate VP39-VP55 Protein Heterodimer

Akihiro Oguro,[2] Lela Johnson, and Paul D. Gershon[1]
Department of Medical Biochemistry and Genetics/Institute of Biosciences and Technology
Texas A&M University System Health Science Center
Houston, Texas 77030

Summary

VP39 is a vaccinia virus-encoded RNA modifying protein with roles in the modification of both mRNA ends. At the 3′ end it acts as a processivity factor for the vaccinia poly(A) polymerase (VP55), promoting poly(A) tail elongation. Despite VP39's three-dimensional structure having been elucidated along with details of its mode of mRNA 5′ end binding, the VP39-VP55 heterodimer's molecular mechanism of processivity is largely unknown. Here, the area immediately above almost the entire surface of the VP39 subunit was probed using chemical reporters, and the path of a previously unidentified RNA binding site was revealed. The path was indicated to fall within a cleft formed by the intersubunit interface and was consistent with both a previously reported model of the heterodimer-nucleic acid ternary complex and the known function of the heterodimer in processive poly(A) tail elongation.

Introduction

VP39 is a multifunctional vaccinia virus protein with roles in the modification of both mRNA ends. At the 5′ end it acts catalytically as a cap-specific mRNA 2'-O-methyltransferase which converts the mRNA cap 0 structure (m^7GpppN…) to its cap I (m^7GpppNm…) counterpart [1, 2]. At the mRNA 3′ end, VP39 apparently acts stoichiometrically, as a processivity factor for the vaccinia poly(A) polymerase (PAP) VP55 [3], with which it forms a heterodimer [4, 5]. VP39 may also have a third function, namely, the control of transcript-length homeostasis, at the transcriptional level [6]. VP39's high-resolution crystal structure has been solved as a complex with its methyltransferase cofactor (*S*-adenosyl methionine) and with cofactor-product (*S*-adenosyl homocysteine) plus 5′ capped RNA substrate [7–10]. Although these data along with supporting mutagenesis [8–11] have proven extremely informative with respect to VP39's 5′ end-modifying function, they have shed little or no light upon VP39's function at the mRNA 3′ end, largely because (1) mRNA 3′ end-related nucleic acid ligands such as uncapped poly(A) have not been successfully cocrystallized with VP39; (2) among the many tens or even hundreds of VP39 mutants that have been generated [2, 11, 12], only one has yet been identified that is specifically defective in PAP-processivity activity [12]; (3) no crystal structure is available for VP55; and (4) VP39 shows no significant sequence similarity to nonpoxvirus proteins.

For VP39's 3′ end-modifying function, the functionally relevant entity would be a ternary complex of VP55, VP39, and the mRNA 3′ end. A stable model ternary complex for the 3′ end-modification reaction [13], containing VP55, VP39, and a model polyadenylation-specific 50mer oligonucleotide ligand bearing the motif $(rU)_2$-N_{25}-rU (dubbed the "heterodimer binding motif"), can be readily assembled. One macromolecular interaction that undoubtedly occurs within this ternary complex is the dimerization of VP39 and VP55. The VP39-VP55 dimerization interface has previously been localized on the surface of VP39 [12], circumventing the methodological hurdles described above through the use of various molecular and biochemical approaches. Thus, side chains critical for dimerization, dimerization-dependent steric effects, and distance constraints between the two subunits were identified via mutagenesis in combination with a "pull-down" assay, protease footprinting, and a site-specific photocrosslinking assay, respectively; the resulting data were modeled on the VP39 surface [12]. In addition to the dimerization interface, one or both subunits would be expected to interact with the oligonucleotide component of the model ternary complex. Using a photosensitive analog located at position −10 with respect to the oligonucleotide 3′ end, a side chain of VP39 has been identified that forms a zero-length photocrosslink with the downstream rU of the heterodimer binding motif of the oligonucleotide component [13]. This indicates that, within the ternary complex, VP39 interacts directly with the −10 region. Moreover, the location of the photocrosslinked side chain on the VP39 surface indicated that VP39 possesses an RNA binding site that is distinct from the crystallographically characterized cleft that docks with the capped mRNA 5′ end. Consistent with this, other studies have indicated the possession by VP39 of two distinct RNA binding sites, only one of which shows cap specificity [14]. Thus, VP39 appears to possess distinct RNA binding sites for its 5′ and 3′ end mRNA-modifying functions, with the latter site lying close to, or within, the VP55-dimerization interface [13]. It was not clear from these preliminary experiments whether the mRNA 3′ end is completely enclosed ("clamped") within a "channel" running through the subunit interface, or simply bound very close to one side of the interface.

In addition to the above physical data, recent oligonucleotide selection and photocrosslinking studies have led to a conceptual model of the overall topology of a VP55-VP39-model oligo ternary complex [15], whose salient features are as follows: (1) the minimum oligonucleotide size that stably binds the VP55-VP39 heterodimer (45 – 50 nt) is 10 nt longer than that for monomeric VP55 (35–40 nt) [13, 16]. This is because the presence of VP39 "shifts" VP55's optimal $(rU)_2$ contact point in the bound oligo from nucleotides −26, −27, with respect

[1]Correspondence: pgershon@tamu.edu
[2]Present address: Department of Tumor Biology, The Institute of Medical Science, The University of Tokyo, Tokyo, Japan, 108-8639.

to the 3′ end, to nucleotides −36, −37. Therefore, the optimized oligonucleotide ligands for VP55 and for the heterodimer possess the motifs $(rU)_2$-N_{15}-rU and $(rU)_2$-N_{25}-rU, respectively. (2) The 3′ half of the heterodimer binding motif-bearing oligonucleotide contacts both subunits, apparently tracking close to the intersubunit interface. (3) While the downstream rU of the heterodimer binding motif (falling within the 3′ half of the oligonucleotide) contacts both VP39 and VP55, the upstream $(rU)_2$ portion contacts VP55 alone.

An overall understanding of the macromolecular contacts within the ternary complex would be of great value in identifying the path of the mRNA 3′ end across the VP39 surface, the relationship between the mRNA 3′ end binding site and the dimerization interface, and the physical reason for the 10 nt shift in VP55-oligonucleotide contact point in the context of the heterodimer. Given the relatively long "minimum-length" of oligonucleotide that is required for heterodimer binding (~50 nt, of which at least approximately the entire 3′ half apparently interacts with the VP39 subunit [15]), we felt that an approach that addresses the entire subunit surface was required. Since high-resolution structural approaches are still beyond reach for the ternary complex, we have applied a site-specific photocrosslinking technique that was successfully used in the identification of the VP55-VP39 dimerization interface [12] (above), but on a more comprehensive scale. A comprehensive single-cysteine mutant library was generated and applied in the generation of photocrosslinking data along with additional site-specific assays. Taken as a whole, the data revealed the path of an mRNA polyadenylylation-related RNA binding site on the VP39 surface, enclosing the side chain previously shown to form a zero-length photocrosslink with the heterodimer binding oligonucleotide ligand. Part or all of the newly characterized RNA binding surface apparently lies within a cleft formed at the interface between VP39 and VP55, whose properties may account for VP39's function as a processivity factor. Moreover, the path of the RNA over the VP39 subunit shows the potential to template a "kink" into the bound RNA, which might account for the 10 nt shift in VP55-RNA contact position in the context of heterodimer. The data correlate well our published conceptual model of the ternary complex [15].

Results

Single Cysteine Mutants of VP39

Wild-type VP39 possesses two cysteine residues, located at positions 178 and 272 in the linear sequence. VP39's 2′-O-methyltransferase and PAP processivity functions are not affected by serine substitution of the two cysteines either individually or together [2]. Using the doubly substituted ("cysteine-minus") mutant (C178S/272S) as a template, a number of additional single-cysteine substitution mutants have been constructed [12]. At the outset of the current study, we extended this process by designing a "library" of single-cysteine substitution mutants. Each cysteine was placed at a position on the VP39 surface which, when forming the center of a 15 Å radius sphere, led to a series of spheres contacting one another close to the VP39 surface with a minimum of intervening space. To identify optimal cysteine positions, we took as a starting point one of the two singly substituted cysteine mutants of [2] (we chose mutant C178S because in the other mutant, C272S, the Cys178 side chain is almost entirely buried and cannot be derivatized efficiently [12]) along with the three single-cysteine mutants of Shi et al. [12] (R55C, R107C, F115C). From this starting point, the above analysis (followed by a confirmation that the thiol of the cysteine substitution would be likely to be solvent accessible), suggested that cysteine substitutions additionally be made at residues F13, E29, P71, Y77, Y83, K126, Q183, Y189, E217, N255, F265, and F293, and that mutant C272S was redundant. Figure 1A indicates the patches of VP39's water-impenetrable surface that are enclosed by the 15 Å spheres, with each one shown as a distinctly colored patch.

The sixteen mutants of the library (F13C, E29C, R55C, P71C, Y77C, Y83C, R107C, F115C, K126C, C178S, Q183C, Y189C, E217C, N255C, F265C, and F293C) were individually expressed in *E. coli*, and the recombinant proteins were purified. The Coomassie-stained gel of Figure 1B shows that each could be obtained in acceptable yield and purity. In the electrophoretic mobility shift assay (EMSA, Figure 1C), each of the 16 mutants was able to form a ternary complex with VP55 plus a 50mer oligonucleotide bearing the $(rU)_2$-N_{25}-rU heterodimer binding motif (the same oligo referred to as "UU$(dC)_{25}$U" in Figure 2B of ref. [13]). The ability of each mutant to form a complex with VP55 and oligonucleotide indicated that none of the single-cysteine substitutions grossly affected VP39's macromolecular binding properties.

Site Specific Photocrosslinking Assay

As an initial approach to exploring the topology of the VP39-VP55-oligonucleotide ternary complex, we used a site-specific photocrosslinking assay to identify regions of VP39 that are proximal to VP55 within the VP55-VP39 binary complex. This assay, which was initially formulated by the Ebright lab [17], was implemented as described in [12]. Thus, a ^{125}I-labeled version of a site-specific photocrosslinker, *S*-[2-(4-Azidosalicylamido) ethylthio]-2-thiopyridine (AET), was attached to the unique cysteine of each mutant by disulfide exchange followed by assembly of the derivatized VP39 mutants into binary complexes with VP55, brief UV irradiation of the complexes and SDS-PAGE. As found previously [11], mutant C178S/272S could not be labeled with ^{125}I-AET, consistent with the absence of cysteines therein (data not shown). In addition, treatment of ^{125}I-AET-derivatized mutants with reducing agent led to a complete loss of label (data not shown), confirming thiol-specificity in the site of AET attachment. Figure 2A shows the data for each mutant. A band corresponding to photocrosslinked VP55-VP39 heterodimer has previously been shown to form after mixing AET-derivatized versions of either R55C, R107C, or C178S with VP55 followed by UV irradiation [12]. Herein, an equivalent band was detected for these three mutants and also for nine others (see Figure 2A, lane 4, for each of the mutants; data summarized in Table 1, column 2). As previously [12], the

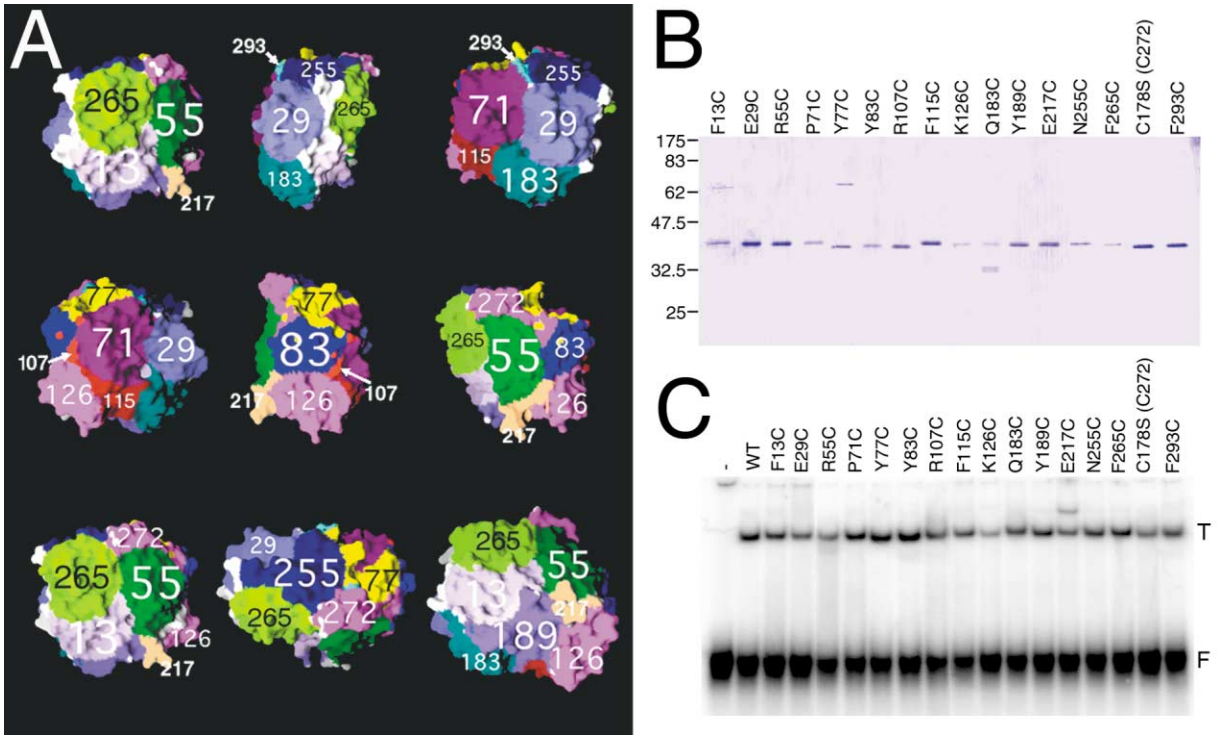

Figure 1. Design, Expression, and Functionality of the Single-Cysteine Mutant

(A) Views of VP39's water-impenetrable surface, generated using the program GRASP [25], through which invisible 15 Å radius spheres have been projected. Each sphere is centered upon one of the sixteen side chains that was substituted with cysteine in this study, and patches of surface enclosed within the spheres have each been given a different (arbitrary) color. The dominant color within each of the overlapping regions is also arbitrary. Numbers within each patch denote the surface residue upon which the sphere was centered (and which was substituted with cysteine in this study). Upper two rows: rightward rotations about the *y* axis through 360° (right-most view on upper row corresponding to VP39's cleft face containing the methyltransferase catalytic center). Lower row: Left-most view corresponds with same on upper row, second and third views are 90° rotations about *x* axis (downward and upward, respectively).

(B) Composited Coomassie-stained SDS-PAGE gels showing the sixteen single-cysteine mutants. After running this gel and prior to subsequent experiments, protein amounts were normalized with respect to one another.

(C) EMSA gel showing ternary complex formation by each of the sixteen mutants and also by wild-type VP39 (i.e., VP39-ΔC26, the fully functional C-terminal truncation mutant after expression in *E. coli* as described [26]). "F" indicates the free oligo, "T" indicates the VP55-VP39-oligo ternary complex. The complex was clearly distinguishable as ternary both from its relative mobility and insofar as neither free VP55 nor free VP39 bind this probe with sufficient stability to be visible after nondenaturing gel electrophoresis ([13] and [14], respectively).

band identified as corresponding to photocrosslinked subunits was UV dependent (for UV-minus control, see Figure 2A, lane 3 for each mutant), implicating AET's photoreactive aryl azide moiety.

To assay for VP55-dependent VP39-oligonucleotide photocrosslinking, a distinct site-specific photocrosslinking assay was developed in which the 16 mutants were first derivatized with unlabeled AET, then UV irradiated in the presence of ^{32}P-labeled oligo UU-(dC)$_{25}$-U in either the absence or presence of VP55 (Figure 2B). For 14 of the 16 mutants, photocrosslinked adducts between VP39 and oligo UU-(dC)$_{25}$-U were detected in either the absence or presence of VP55 or both (Figure 2B, lanes 4 and 6 for each mutant; data summarized in Table 1, column 3). The assay shown in Figure 2B was repeated, and the photocrosslinked band was quantitated for each mutant in each of the duplicate assays. Mean fold enhancements in VP39-oligo photocrosslinking due to the presence of VP55 are plotted in Figure 2C where, due to the log scale, positive values indicate VP55-induced enhancement of ternary complex formation (more specifically, ternary complex-dependent photocrosslinking, since VP55 is one of the three defining components of this complex). A 2-fold or greater enhancement (above the gray area in Figure 2C) was considered to be significant. Such an enhancement was observed for eight of the mutants (as summarized in Table 1, column 3). It is not known why ternary complex-nonspecific crosslinking is high for some mutants; however, the previously well-characterized methyltransferase-specific "cleft" binding site for capped mRNA 5′ ends is known to have some weak activity in the binding of uncapped RNA [14], which could lead to the covalent trapping of oligo during the photocrosslinking assay. Of the six mutants with detectable photocrosslinking activity that is not VP55-enhanced (E29C, P71C, F115C, Y189C, E217C, and F265C), the former three are arrayed around the cleft.

In Figure 3, the data of Figure 2 are projected onto the VP39 surface. Evidently, the newly characterized VP39-RNA proximal regions found within the ternary complex form a previously uncharacterized, contiguous

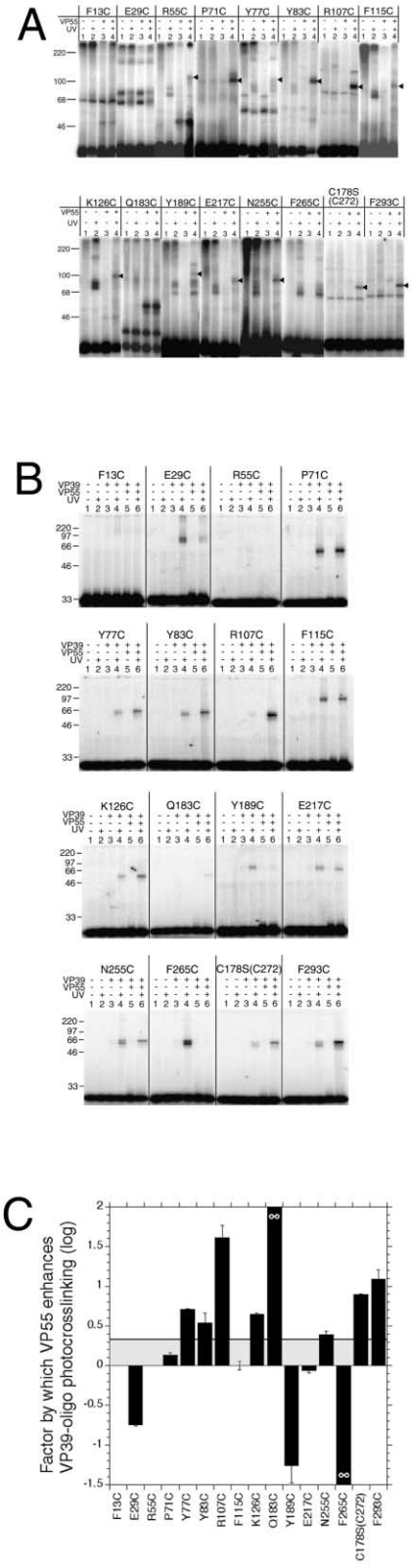

Figure 2. Photocrosslinking Data

(A) VP39 mutants derivatized with ^{125}I-labeled AET: photocrosslinking to VP55 within VP55-VP39(mutant) binary complexes. The composite images of storage phosphorgrams of SDS-PAGE gels show site-specific photocrosslinking products for ^{125}I-AET-derivatized versions of each of the VP39 single-cysteine mutants in the presence or absence of VP55 and UV irradiation. The abundant band at the bottom of each gel corresponds to the labeled VP39 mutant. Arrowheads indicate bands corresponding to ^{125}I-labeled photocrosslinked VP39-VP55 heterodimer. Minor contaminating proteins in the VP39 mutant preparations have become derivatized to a variable extent. VP55 has also become derivatized in some experiments, due to difficulties removing all of the unreacted ^{125}I-AET after VP39 derivatization. However, specific photocrosslinking products were clearly identifiable on the basis of both electrophoretic mobility and the combination of experimental factors (UV light, other macromolecules present, as indicated by +/−). To support the validity of our assignments, each of the controls described in [12] was repeated here (data not shown). The approximate migration positions of ^{14}C-labeled protein standards are indicated to the left of each panel. The migration positions are approximate insofar as the figure is a composite from more than one gel.

(B) VP39 mutants derivatized with unlabeled AET: photocrosslinking to ^{32}P-labeled oligonucleotide in the presence and absence of VP55. Storage phosphorgrams of SDS-PAGE gels show site-specific photocrosslinking products for ^{32}P-labeled oligo UU-(dC)$_{25}$-U in the presence or absence of unlabeled AET-derivatized versions of each of the VP39 single-cysteine mutants, VP55, and UV irradiation. The abundant lower band in each gel corresponds to free oligo. The approximate migration positions of ^{14}C-labeled protein standards are indicated to the left of each panel. The migration positions are approximate insofar as the figure is a composite from several different gels. For mutant Q183C, the electrophoretic mobility of the crosslinked species corresponded exactly to that of other crosslinked single-cysteine mutant samples run in the same gel (e.g., the adjacent K126C samples), indicating that crosslinking of full-length Q183 protein was detected as opposed to that of the ~32 kDa contaminant visible in Figure 1B.

(C) Band intensities in the storage phosphorgrams of (B) and a duplicate experiment (data not shown) were quantitated, and mean values were calculated for each mutant. The ordinate (factor by which VP55 enhances VP39-oligo photocrosslinking [log]) indicates log transformations of the mean intensity of the photocrosslinked band in the presence of VP55 (lane 6 of panel [B] or replicate experiment)/intensity of the photocrosslinked band in the absence of VP55 (lane 4 of panel [B] or replicate experiment). Via the log transformation, only mutants showing VP55 enhancement of photocrosslinking score positive, a value of "1" representing one order of magnitude. Error bars denote the two individual values (only one of the two error bars being visible in most cases). The horizontal line at factor = 2 ($\log_{10}$factor = 0.3) represents the designated threshold for significant ternary complex-specific photocrosslinking (the area below this line is colored gray). For each of the positive-scoring single-cysteine mutants, values for both of the two contributing replicate experiments were above the threshold also. Where a pair of closely spaced bands for the VP39-oligo photocrosslinked complex in the absence of VP55 was clearly discernible and was converted to a single band in the presence of VP55 (e.g., for mutants Y77C, E217C, N255C, C178S, F293C, [B]), only the relevant member of the pair contributed to the quantitation shown in (B).

RNA binding site running across one surface of VP39. Being ternary complex specific, this site is presumed to act in VP39's PAP processivity function. A previously mapped ternary complex-specific, RNA-contacting side chain (R107 [13]) is enclosed within the newly characterized site. The new site appears to be entirely distinct from either the crystallographically defined methyltransferase-specific cleft [9] or the symmetry-related contact site for the 3′-most base of the cocrystallized ligand that occurs on the reverse face of VP39 from the cleft [9]. Interestingly, the newly characterized RNA binding site appears to either run through the center of, or be straddled by, VP39's dimerization interface for VP55.

Table 1. Summary of Data Elucidated Herein

Mutant	Crosslink to VP55 (Figure 2A)	VP55-Enhanced Crosslink to Oligo (Figures 2B and 2C)	Thiol Occlusion, VP55 (Figures 4D–4F)	Thiol Occlusion, VP55 + oligo (Figures 4D–4F)	FeBABE (Figure 5)
F13C		N	▼▼	◀▶	
E29C		▼	◀▶	◀▶	•
R55C	•	N	▼	◀▶	
P71C	•	◀▶	◀▶	▼	•
Y77C	•	▲	U	U	
Y83C	•	▲	▼	▼	
R107C	•	▲	▼	▼	
F115C	•	◀▶	◀▶	◀▶	
K126C	•	▲	◀▶	◀▶	
Q183C		▲	◀▶	◀▶	
Y189C	•	▼	◀▶	◀▶	
E217C	•	▼	◀▶	◀▶	
N255C	•	▲	▼▼	▼	
F265C		▼	▼	◀▶	
C178S(C272)	•	▲	▼▼	▼	
F293C	•	▲	▼	▼	

Crosslink to VP55 (column 2): •, UV-dependent VP55-dependent intersubunit photocrosslink detected. VP55-enhanced crosslink to oligo (column 3): N, none detected; ◀▶, unaffected by presence of VP55; ▲, significantly enhanced in presence of VP55, ▼, diminished in presence of VP55. Thiol occlusion (columns 4 and 5): U, unreactive; ◀▶, unoccluded; ▼▼, partially occluded; ▼, occluded. FeBABE (column 6): •, FeBABE-dependent oligo cleavage observed.

Thiol Occlusion Assay

To complement the photocrosslinking (proximity) data (above), we aimed to identify surface regions of VP39 remaining accessible to solution-phase small molecules after incorporating VP39 into the ternary complex. For this, we synthesized a thiol-specific Cy3 derivative (Cy3-maleimide, Figure 4A). To check for specificity and reactivity, the compound was incubated with each of the 16 single-cysteine mutants and the cysteine-minus control (C178/272S), in the absence of other macromolecules, followed by SDS-PAGE and fluorimaging (Figure 4B). The cysteine-minus mutant (C178S/272S) did not react detectably with Cy3-maleimide (Figure 4B), consistent with its lack of a reactive thiol. With one exception (Y77C), each of the single-cysteine mutants was clearly reactive (Figure 4B) and was further investigated in a reactivity timecourse assay. Reasons for the very low reactivity of Y77C are unclear. As an example of the timecourse assay, Figure 4C shows data for the reaction of Cy3-maleimide with mutant F293C.

Figures 4D–4F show timecourse assay data for each of the reactive single-cysteine mutants, either alone, in the presence of VP55, or in the presence of both VP55 and oligo UU-$(dC)_{25}$-U. VP55 did not significantly affect Cy3-maleimide access to the surface thiols of seven of the reactive mutants (Figure 4D; Table 1, column 4). For three reactive mutants, an intermediate effect was observed in which rates of access were significantly diminished (Figure 4E, Table 1 column 4). Access of Cy3-maleimide to the surface thiols of the remaining five reactive mutants was strongly restricted in the presence of VP55 (Figure 4F; Table 1, column 4).

For mutants P71C and C178S, the presence of oligo UU-$(dC)_{25}$-U led to a significant decrease in thiol accessibility (Figures 4D–4F; Table 1, column 5), in which significance is defined as clearly nonoverlapping error bars between oligo$^+$ and oligo$^-$ reactions. For four additional mutants (Y83C, R107C, N255C, F293C, Figures 4D–4F and Table 1, column 5), the presence of oligo UU-$(dC)_{25}$-U led to a perceptible and reproducible decrease in reactivity whose significance is unclear insofar as error bars represent maximum and minimum values from two experiments only. Nonetheless, error bars in Figures 4D–4F are relatively small despite representing minimum and maximum values, attesting to the reproducibility of the data. We therefore feel it is notable that five of the six mutants whose reactivity was perceived to drop in the presence of oligo UU-$(dC)_{25}$-U (Y83C, R107C, F293C, C178S, and N255C) comprise the complete set of mutants whose unique thiols lie within the newly characterized RNA binding site (Figure 6, below). The unique thiol of the sixth mutant, P71C, lies close to the proposed "entrance" to the RNA binding site (see Discussion). Results were therefore as one might expect to find for residues at the interface of a protein-nucleic acid complex.

Chemical Nuclease Assay

To identify regions of VP39 proximal to oligonucleotide UU-$(dC)_{25}$-U within the ternary complex, we coupled a chemical nuclease, iron (S)-1-(p-bromoacetamidobenzyl)-ethylenediaminetetraacetate (FeBABE), to each of the sixteen single-cysteine mutants, followed by incubation with VP55 and oligo UU-$(dC)_{25}$-U (either 5′ or 3′ end-labeled) in an attempt to form a ternary complex. Site-directed cleavage was initiated using ascorbate and hydrogen peroxide. The resulting hydroxyl radicals were expected to be localized within a 10 Å radius of the iron center [18] which, together with the 12 Å of tether length for FeBABE, would provide a maximum cleavage radius of ~22 Å from the cysteine sulfur (~25 Å from the $\alpha-$carbon). In the first step of this assay, we derivatized the VP39 single cysteine mutants with FeBABE. FeBABE derivatization was monitored in control experiments by following the FeBABE coupling step with a Cy3-malei-

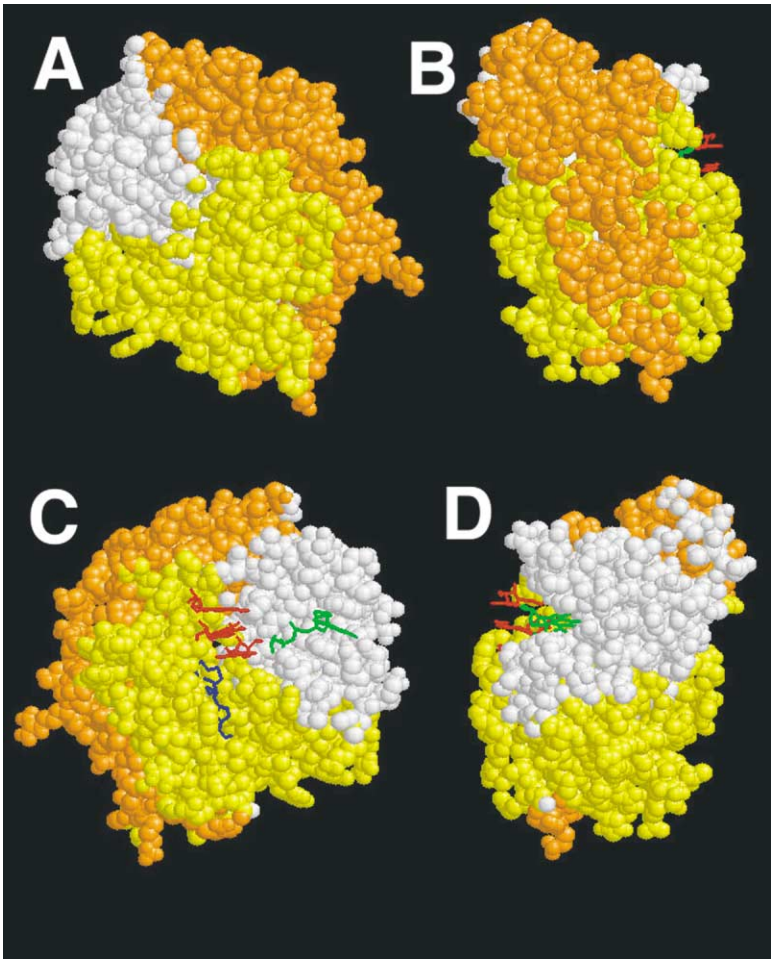

Figure 3. Data from Crosslinking Experiments of Figure 2/Table 1, Projected onto the Crystallographically Defined Surface of VP39

The VP39 surface was rendered (spacefill) using the program RASMOL2 [27] with pdb file 1av6. Leftward 90° rotations are shown, progressing from VP39's reverse face (A) which was previously shown to possess strong dimerization contacts [12] through the side face (B) and front face (C). The m^7GpppGpApA portion of the cocrystallized hexameric methyltransferase substrate RNA [9] and the *S*-adenosylhomocysteine methyltransferase cofactor product are shown in stick rendering in (C). Green and red sticks represent m^7Gppp cap and GpApA portions of the RNA, respectively; blue stick represents AdoHcy. Brown: Surface atoms located within 15 Å radius spheres centered upon the side chains of those AET-derivatized single-cysteine mutants able to photocrosslink with both VP55 and oligo. Yellow: Surface atoms located within 15 Å radius spheres centered upon the mutated side chains of single-cysteine mutants that are AET photocrosslinkable to VP55 but not oligo. All other surface atoms are uncolored (white). Yellow regions were rendered after brown regions, so that areas which are unable to photocrosslink to the oligo are dominantly defined. Since the role of the 3D structures is to indicate topological considerations alone, the variability in crosslinking efficiency that is apparent in Figure 2 is not indicated in the figure.

mide incubation step. In these experiments, FeBABE-derivatization followed by extensive dialysis to eliminate free FeBABE completely blocked the subsequent coupling of Cy3-maleimide to the VP39 mutants (data not shown), indicating a high efficiency of FeBABE coupling. In other control experiments, each of the mutant proteins could be derivatized with FeBABE as monitored using ^{55}FeBABE [19]. However, after combining the ^{55}FeBABE-labeled VP39 single-cysteine mutants with VP55 and oligo UU-$(dC)_{25}$-U and subjecting the mixtures to the EMSA, ternary complexes were found to be destabilized by prior FeBABE derivatization of the mutant proteins (data not shown). This may arise from the bulky and ionic nature of the FeBABE reagent with respect to other cysteine-derivatization reagents used herein, along with its longer reach.

It was considered that, although sensitive to EMSA gel analysis, FeBABE-VP39/VP55/oligo ternary complexes might be sufficiently stable to attempt chemical cleavage analysis. Thus, FeBABE-derivatized VP39 single-cysteine mutant proteins were mixed with oligo and VP55 followed by incubation with peroxide and ascorbate, and electrophoresis of the oligonucleotide products in polyacrylamide-urea gels. Specific signals were observed for only 2 of the 16 mutants, namely, E29C and P71C, and were observed using either 5′ or 3′ end-labeled oligo (Figures 5A and 5B, lanes 9, 10 and 10, 11, respectively; Table 1, column 6). The specific cleavages were at oligo positions −17 to –28 for the two derivatized mutants. After quantization of the electropherograms obtained for cys-minus, E29C and P71C (Figure 5A, B, lanes 9, 10 and 10, 11), followed by subtraction of the average quantized signal for the 14 negative mutants (data not shown), cleavage nodes were clearly apparent for E29C and P71C in contrast to cysteine-minus (plotted to the left of electropherograms, Figure 5). In control incubations of oligo with FeBABE-underivatized cysteine-minus, E29C, or P71C, or derivatized versions in the absence of ascorbate/peroxide, only uniform background levels of cleavage products were observed at low abundance (Figures 5A and 5B, lanes 2–7 and 3–8, respectively), indicating that the observed nodes were a result of specific chemical cleavage. Other controls indicated an absence of cleavage activity associated with VP55 (data not shown). Finally, the absence of specific cleavage nodes upon omission of VP55 but in the presence or absence of peroxide/ascorbate, (data not shown) indicated that the cleavage nodes for E29C and P71C were ternary complex specific.

The E29 and P71 mutation sites are positioned fairly close to one another on the VP39 surface (Figure 6). Interestingly, despite the ability of FeBABE-derivatized versions of mutants E29C and P71C to cleave oligo UU-$(dC)_{25}$-U within the ternary complex, AET-derivatized

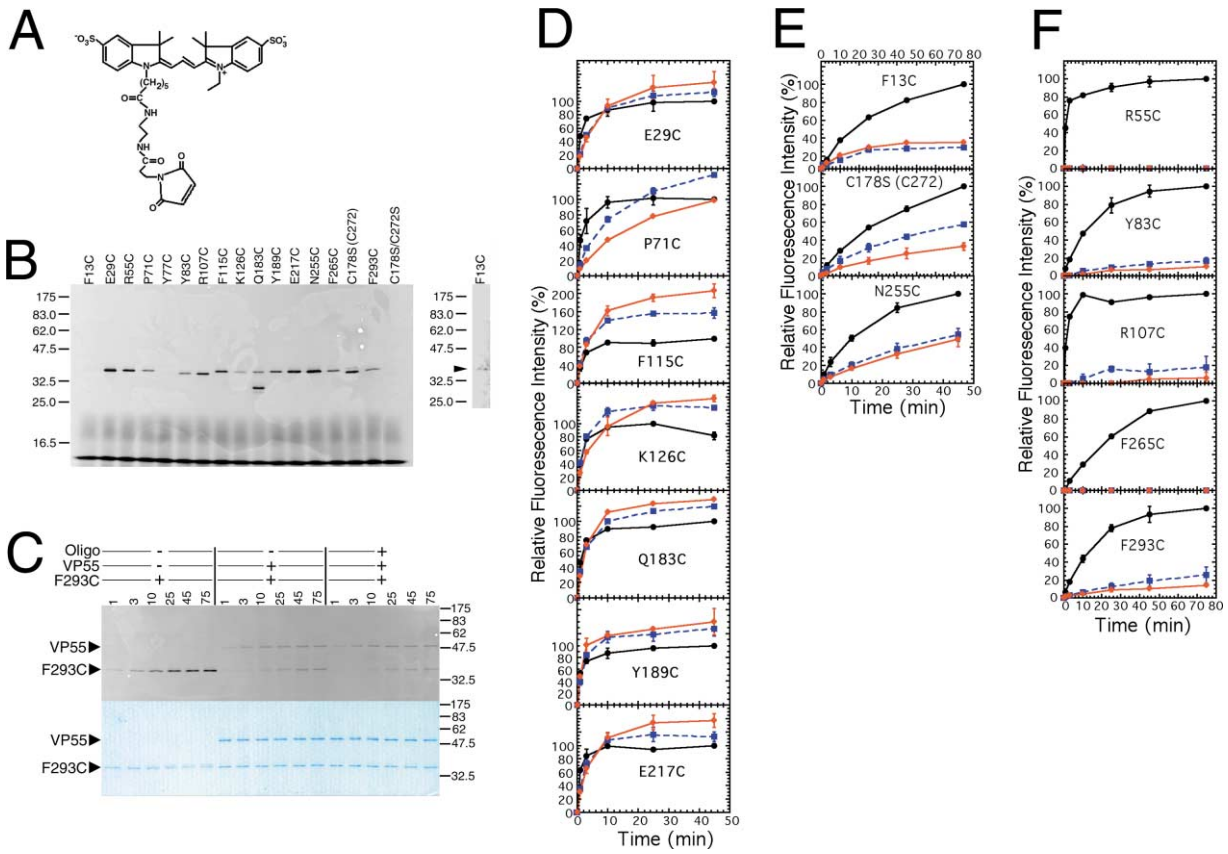

Figure 4. Development and Implementation of the Thiol-Occlusion Assay

(A–C) Development of the assay. (A) Molecular structure of Cy3-maleimide, as synthesized herein. (B) Fluorimage of SDS-PAGE gel showing the reactivity of each of the sixteen single-cysteine mutants with Cy3-maleimide in the absence of other macromolecules. The migration positions of protein standards are indicated to the left. "C178S/C272S" denotes the cysteine-minus mutant. Fluorescence for F13C, although barely visible in the main panel, was visible upon increasing contrast (right panel). (C) Reactivity timecourse data for mutant F293C in the absence of other macromolecules. Upper panel: Fluorimage of SDS-PAGE gel showing samples taken at various times (1–75 min) after mixing mutant F293C with Cy3-maleimide in the presence/absence of VP55 and oligo UU-$(dC)_{25}$-U. VP55 reactivity indicates that it has free thiols. Lower panel: Subsequent Coomassie stain of the same gel (showing that each lane contains equivalent amounts of F293 protein). The migration positions of protein standards are indicated to the right.

(D–F) Thiol occlusion assay data. Plots show relative fluorescence intensity versus time of reaction with Cy3-maleimide for 15 of the 16 VP39 single-cysteine mutants either alone (●), in the presence of VP55 (binary complex, ■), or in the presence of both VP55 and oligo UU-$(dC)_{25}$-U (ternary complex, ◆). Y77C could not be tested because its reactivity with Cy3-maleimide (B) was insufficient for detection in the timecourse assay. Ordinate: Fluorescence intensity, as a proportion of the peak intensity observed for the VP39 mutant alone, converted to percent. All assays were performed in duplicate: mean values from duplicate experiments are shown, error bars indicate the individual values. (D) Mutants whose thiols were not occluded after complex formation. (E) Mutants whose thiols were considered to be partially occluded after complex formation, insofar as relative fluorescence intensity was diminished but nonetheless $>25\%$ of that of the uncomplexed mutant by the end of the experiment (upper time scale applies to upper two plots, lower time scale applies to lower plot). (F) Mutants whose thiols were considered to be occluded after complex formation insofar as relative fluorescence intensity was $\leq 25\%$ of that of the uncomplexed mutant by the end of the experiment.

versions of the two mutants were unable to form a ternary complex-specific (i.e., VP55-enhanced) photocrosslink with the oligo (Figures 2B and 2C). Although we cannot discount the possibility that AET-photocrosslinkable groups are absent in the relevant region of the oligo, we consider this unlikely because of the relatively nonspecific photocrosslinking characteristics of AET's reactive aryl azide moiety [20]. Instead, the data may be resolved by considering the differences in "reach" of AET and FeBABE (14 Å and 22 Å from the cysteine sulfur, respectively; i.e., 17 Å and 25 Å, respectively, from the $\alpha-$carbon). We therefore consider it possible that the oligonucleotide "peels away" from the VP39 surface in the vicinity of amino acids 29 and 71, to a distance of between 14 and 25 Å.

A model for the overall topography of VP39, as deduced from the above experiments, is shown in Figure 6.

Discussion

Using various thiol-specific probes, we have charted the area above the surface of VP39 within the VP39-VP55-nucleic acid ternary complex and thereby gained insight into the physical topography of the ternary complex. Figure 6 summarizes the findings.

Two closely apposed regions were previously impli-

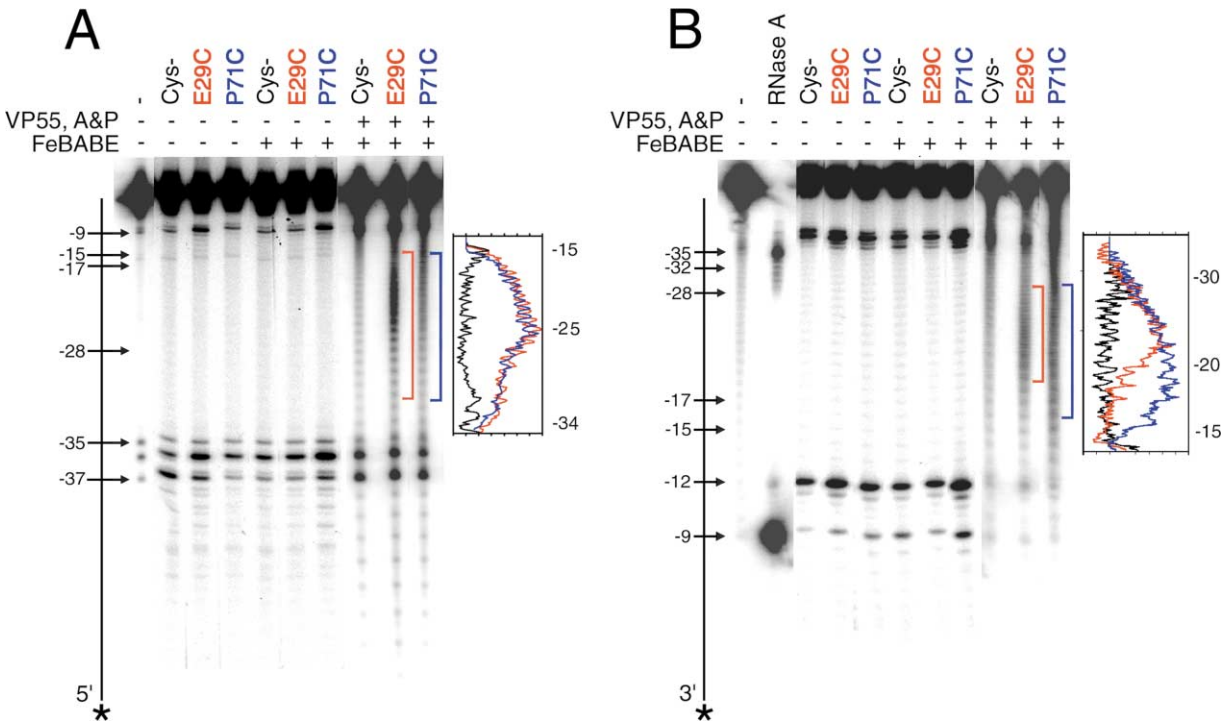

Figure 5. Chemical Nuclease Assay

The figure shows products after incubation of ^{32}P end-labeled oligo UU-(dC)$_{25}$-U with either no protein ("−"), VP39 cysteine-minus mutant ("Cys−") or VP39 single-cysteine mutants E29C and P71C. "FeBABE" denotes use of derivatized protein; "A&P" denotes presence of ascorbate and peroxide. Distances of cleavage sites from the oligo 3′ end are indicated to the left of the two storage phosphorgrams. The plots to the right of each of the two panels show quantitation of the E29C (red) and P71C (blue) gel lanes, after subtraction of the corresponding values for the Cys− gel lane values from each. As an indication of significance, the average signal for all single-cysteine mutants other than E29C and P71C (gel data not shown) was also subjected to subtraction of the Cys− gel lane data, and the resulting values also plotted (black). Data with derivatized versions of the remaining fourteen single-cysteine mutants were negative in this assay (i.e., resembled the Cys− control, data not shown). For mutant Q183C, this may have been due to low reactivity with FeBABE (data not shown). (A) 5′ end-labeled oligo; (B) 3′ end-labeled oligo. In (B), RNase A partial (almost complete) cleavage products (second lane) were coelectrophoresed as fragment size-markers.

cated in VP39-VP55 dimerization contacts through a combination of mutagenesis, protease footprinting, and preliminary site-specific photocrosslinking experiments [12]. The two regions (on VP39's "reverse" face) were centered on the region around R55/C272, and the region around R107. Both of these two regions are encompassed by the portion of the yellow patch visible in Figures 3A and 3B and Figures 6A and 6B. Not only did the four single-cysteine mutants within this region (R55C, Y83C, R107C, C272) all support cysteine-dependent photocrosslinks with VP55 (Figure 2A; Table 1), but their thiols were also occluded by dimerization with VP55, with three of them being strongly occluded (Figures 4E and 4F; Table 1). This reinforces the notion that this part of the VP39 surface is sequestered within the dimerization interface. It is possible that the region extends upwards to the side chain of F265, insofar as the F265C thiol is strongly occluded by VP55 (Figure 4F; Table 1). However, the F265C thiol did not support photocrosslinking, presumably due to the absence of a crosslinkable group or effects of the AET photocrosslinker on VP55. The subunit interface apparently "opens up" in the region adjacent to (beneath) the R55C, Y83C, R107C, C272 dimerization "patch." Thus, despite the thiols in the adjacent region (i.e., those of mutants Y189C, E217C, K126C) being VP55 photocrosslinkable, they were not occluded from small-molecule derivatization (Figure 6A).

We observed site-specific photocrosslinking of VP39 to both VP55 and the complexed oligonucleotide occurring in a "stripe" running across one side of VP39 (colored brown in Figures 3B and 6B). This stripe seems to indicate the path of binding of the polyadenylylation-specific oligonucleotide within the ternary complex. This previously uncharacterized RNA binding site, which presumably acts exclusively in VP39's mRNA 3′ end formation function, is entirely distinct from the site of binding of the capped mRNA 5′ end. The latter is already known to bind VP39's "front" face (Figures 3C and 6C), as deduced from the X-ray crystal structure of the VP39-capped RNA complex [9]. The possession by VP39 of distinct RNA binding sites for the mRNA 5′ and 3′ ends is consistent with previous biochemical studies indicating the presence of more than one RNA binding site on the VP39 surface [14]. Moreover, the newly characterized site encompasses a residue (R107) that is known to form a strong zero-length photocrosslink with the downstream rU of the (rU)$_2$-N$_{25}$-rU heterodimer binding motif within the standard 50mer oligonucleotide, after substituting this rU with the photosensitive nucleoside ^{4S}rU

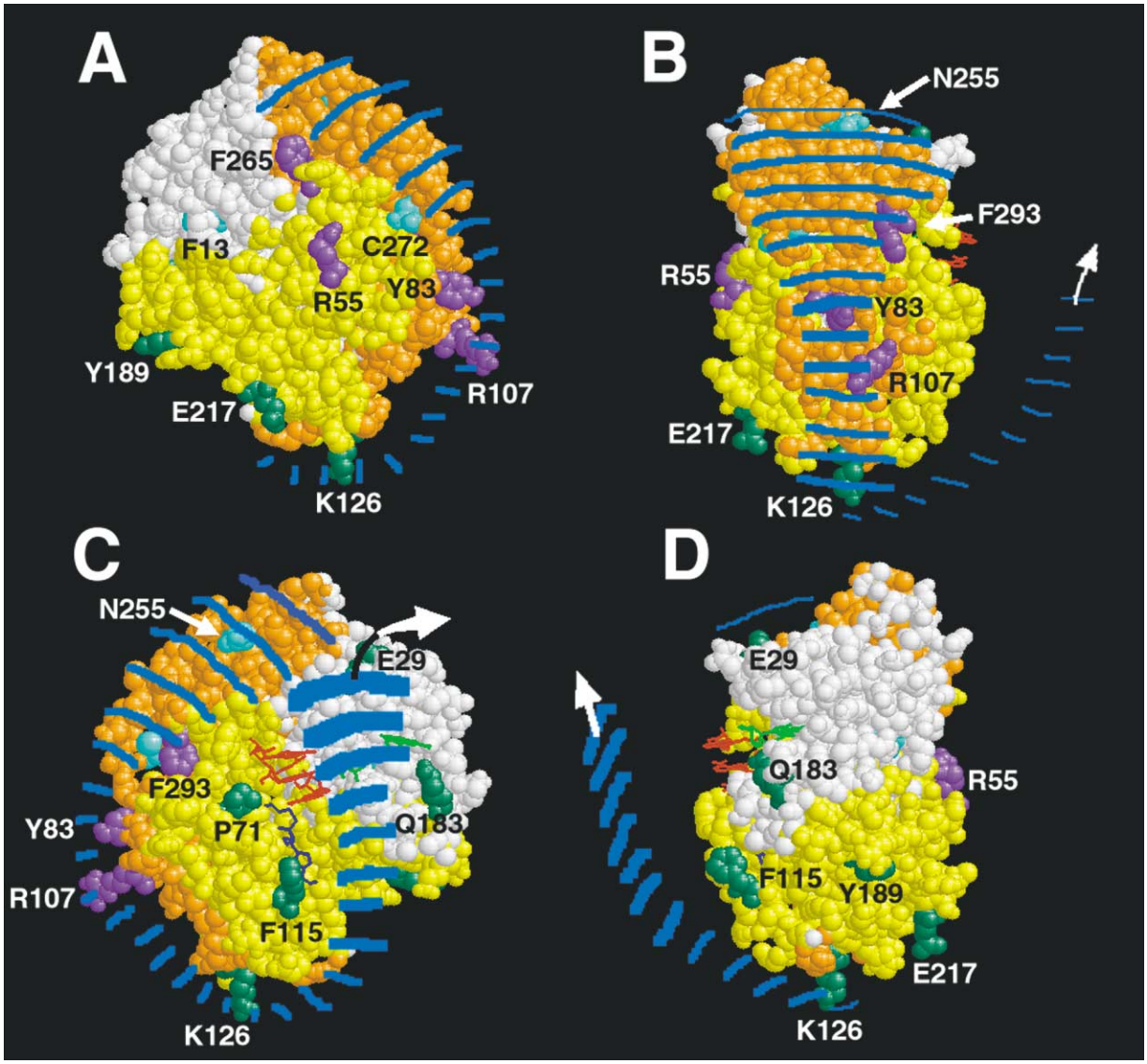

Figure 6. Leftward Rotations of the VP39 Surface Summarizing all the Topographical Data Elucidated Herein and Summarized in Table 1

The overall representation and yellow and brown surface atoms are colored according to Figure 3. In addition, side chains whose cysteine substitution provided VP55-occludable (or VP55 + oligo-occludable) thiols are colored purple, side chains whose cysteine substitution provided nonoccludable thiols are colored green, and those whose substitution provided partially occludable thiols are colored light blue (according to the data of Figure 4, panels D - F). The Y77 side chain is not colored because it was insufficiently reactive with cy3-maleimide to be subjected to the thiol-occlusion assay (see text). Although the unique thiols of mutants Y83C, R107C, and F293C are colored purple, i.e., considered essentially unreactive, they showed a very slight yet reproducible reactivity, which decreased slightly in the presence of oligo (Figure 4F). This is consistent with an occlusional effect of oligo binding (see Discussion). The approximate position of the bound oligo is shown as a blue ladder. Although an outward arrow marks one end of the bound oligo segment, the 5′–3′ polarity of the bound oligo is unknown and therefore is not indicated. Currently, we cannot exclude an alternative model for oligo binding in which it loops over the top of VP39 instead of under the bottom as indicated (see Discussion). Since the role of the 3D structures is to indicate topological considerations alone, the variability in crosslinking efficiency that is apparent in Figure 2 is not indicated in the figure.

followed by ternary complex formation and photoirradiation [13]. The identification of a larger portion of this RNA binding site (herein) greatly extends the previous photocrosslinking data. At the "top" of the newly characterized RNA binding site, thiols are only partially occluded in the VP55-VP39 binary complex and the VP55-VP39-oligo ternary complex (light blue side chains in Figures 6B and 6C), indicating an opening-up of the RNA binding site in this region.

On VP39's front face, to which the capped mRNA 5′ end binds (i.e., to the righthand side of the newly characterized RNA binding site) VP39 and VP55 also photocrosslink to one another within the ternary complex (yellow patch in Figures 3C and 6C). However, thiols are not occluded on the front face (Figure 6C), in contrast to the reverse face (above). This would indicate that the dimerization interface does not entirely "enclose" the bound oligonucleotide within a channel running between

the two subunits. Instead, the oligo would appear to run within a deep cleft close to the subunit interface. The unique thiols of mutants Y83C, R107C, and F293C, although almost completely occluded from small molecule reactivity, appear to be reproducibly more occluded in the presence of the model heterodimer binding oligonucleotide ligand than in its absence (Figure 4F). This contrasts markedly with the behavior of thiols located within the dimerization interface (namely, the thiols of mutants R55C and F265C), which were completely unreactive in either the absence or presence of oligo (Figure 4F). Interestingly, the side chains of the former three residues (Y83C, R107C, and F293C) lie precisely in the projected path of the oligonucleotide at the protein surface (Figure 6B), i.e., within the proposed intersubunit cleft containing the newly characterized RNA binding site (Figure 6B). These are the three thiols that would be expected, according to the cleft model, to be the most sensitive to the presence of oligonucleotide. Further support for the cleft model comes from previous photocrosslinking studies [15] in which an azidophenzcyl bromide photocrosslinker was attached at various backbone phosphates to a set of oligonucleotides (each via a unique phosphorothioate), followed by ternary complex formation and photoirradiation. This study showed a node of protein photocrosslinking for APB-attachment points lying between positions –11 and –21 in the oligonucleotide [15]. Since the nodes of photocrosslinking were superimposable for the two subunits, it was surmised that this portion of the oligonucleotide was bound close to the dimerization interface [15], supporting the current cleft model.

In our conceptual model of the topology of the VP55-VP39-standard 3′ end 50mer oligonucleotide ternary complex ([15], see also Introduction), approximately the 3′ half of the oligonucleotide [containing the downstream rU of the $(rU)_2$-N_{25}-rU heterodimer binding motif] interacts with both subunits of the VP39-VP55 heterodimer, while the 5′ portion [containing the upstream $(rU)_2$ portion of the motif] contacts the VP55 subunit alone. The spacing between the two rU-containing patches of the heterodimer binding motif are 10 nt greater than in the $(rU)_2$-N_{15}-rU motif which binds monomeric VP55. By default, this is due to the presence of VP39. The newly characterized RNA binding site indicates a physical path for the 3′ portion of the heterodimer binding motif-containing oligonucleotide (Figure 6). How do our data account for the increased distance between the two rU portions of the motif in the presence of the VP39 subunit? The data of Figure 5 indicate that FeBABE-derivatized mutants E29C and P71C cleave the oligonucleotide between positions –17 and –28, providing a tentative distance constraint for this portion of the bound oligo, namely 14 Å–25 Å above a portion of the VP39 front surface (containing residues E29 and P71). In the context of such a constraint, the oligonucleotide may track through the newly characterized RNA binding site, under the bottom of VP39 (as oriented in Figure 6), then away from VP39's front face which contains the unique thiols of mutants E29C and P71C. Currently, we cannot exclude an alternative model of oligo binding that might also account for the data, in which it loops over the top of VP39 instead of under the bottom. We suggest that the "wrapping" of the oligo under the bottom (or over the top) of VP39 and its exit from the front surface may account for the 10 nt additional spacing between the two rU-containing portions of the oligonucleotide motif in the presence of VP39. In the absence of the VP39 subunit, the segment of RNA between the downstream rU and the upstream $(rU)_2$ would no longer be obliged to wrap around VP39, but might instead remain physically linear after VP55-RNA interaction, leading to the reduced intervening distance between the downstream rU and the upstream $(rU)_2$.

Significance

In this paper, by assaying chemical reporters attached to the unique thiols of a coherent library of single-cysteine mutants, we have probed the space immediately above virtually the entire surface of the vaccinia virus-encoded RNA-modifying protein VP39 (a PAP processivity factor), after assembly of the latter into a ternary complex with the PAP and an oligonucleotide ligand. In doing so, we have located a previously unknown RNA binding site on the protein surface. To our knowledge, an RNA binding site has not previously been identified and characterized in this manner. It's characteristics (i.e., apparently deep cleft at the interface with the vaccinia virus PAP), are consistent with VP39's role in conferring processivity to the PAP.

Experimental Procedures

Materials

VP55 was expressed from recombinant baculovirus-infected High Five insect cells and purified as described [12]. Oligonucleotides were synthesized using a Model 392 DNA/RNA synthesizer (Applied Biosystems) using reagents manufactured by Cruachem. All synthetic oligonucleotides were purified by urea-PAGE before use. The sequence of the chimeric 50mer oligonucleotide referred to here as UU-$(dC)_{25}$-U [13] is $(dC)_{13}$-$(rU)_2$-$(dC)_{25}$-rU-$(dC)_9$-rC.

Mutagenesis, Expression, and Purification of VP39

VP39 point mutants were prepared using the chameleon double-stranded site directed mutagenesis kit (Stratagene) as described [12]. The mutagenesis template for all mutants was the plasmid encoding mutant C178S/C272S as a fusion to the C terminus of glutathione *S*-transferase [2]. Proteins were expressed as described [12]. Briefly, 500–6,000 ml cultures of expression plasmid-transformed *E. coli* strain HB101 were grown in superbroth to saturation at room temperature, induced with IPTG for 2.5 hr at room temperature, purified over glutathione-agarose, cleaved with thrombin, and then purified over heparin-agarose as described [12], except that the heparin-agarose column buffer contained 1 mM EDTA in place of 2-mercaptoethanol. Peak fractions from the heparin-agarose column were quantitated by densitometry of Coomassie-stained SDS-PAGE gels (sometimes after ultrafiltration to concentrate the protein) as described [11].

After purification, all proteins were tested for their ability to conjugate with AET. Those which were unable to do so or did so only weakly were incubated for 1 hr with 1.6 mM dithiothreitol followed by four sequential steps of spin gel-filtration chromatograhy (Macrospin P-6 columns, The Nest Group) after first equilibrating spin columns in 10 mM HEPES-NaOH (pH 8.0), 10% (v/v) glycerol, 25 mM NaCl, 1 mM EDTA, 0.01% (v/v) Nonidet P-40 (buffer A).

^{32}P End-Labeling of Oligonucleotides

Oligonucleotides were 5′ end-labeled with ^{32}P using T4 polynucleotide kinase as described [13]. Oligonucleotides were 3′ end-labeled using [α-^{32}P]cordycepin triphosphate, VP55, and VP39, as described

[21, 22]. After completion of all oligonucleotide-labeling procedures, oligonucleotides were sodium acetate/ethanol precipitated and redissolved in DEPC-treated water.

EMSA

The EMSA was performed as described [21]. Briefly, binding reactions contained buffer A and were 0.25 μM in ^{32}P-labeled oligonucleotide and 0.2 μM in each protein, in a total volume of 10 μl. Mixtures were incubated at room temperature for 15 min then applied to pre-electrophoresed 8% (w/v) polyacrylamide/0.5× TBE gels and electrophoresed at 10 V/cm for 2.5 hr. Gels were imaged using a PhosphorImager (Molecular Dynamics).

Site-Specific Photocrosslinking Assay

The site-specific photocrosslinking assay was performed as described [12] with slight modifications. All procedures were performed under stringently dark conditions. For ^{125}I-labeling of AET (Molecular Probes), 15 nMol of dry AET was dissolved in 100 μl of 0.1 M sodium borate (pH 8.4) supplemented with 1–2 nMol of ^{125}I (5 mCi, ~13 μl, DuPont NEN) and 12.9 nMol of KI (4.3 μl of a 3 mM solution in 0.1 M sodium borate [pH 8.4]). The mixture was added to an IODOGEN (Pierce)-coated reaction vial. After agitation at room temperature (30 s), the mixture was quenched by transferring to a vial containing 100 μl of 2 mM tyrosine in 0.1 M sodium borate (pH 8.4) and incubating at room temperature for an additional 10 min. Ten microliters of the resulting mixture (^{125}I-AET) was mixed with 0.1 nMol of purified VP39 mutant in 100 μl of buffer A. After 1 hr at room temperature, protein was separated from small molecules (e.g., free ^{125}I and ^{125}I-labeled AET) by three sequential steps of spin gel filtration chromatography (as described above). The resulting ~100 μl aliquots of labeled protein were stored at −70°C until use. For photocrosslinking assays, 10 μl of ^{125}I AET-derivatized VP39 mutant was mixed with equimolar portions of VP55 and/or oligonucleotide in a 1.5 ml microtube followed by 10 s of 350 nm irradiation at room temperature using a photochemical minireactor (RMR-600, Southern New England Ultraviolet), then SDS-PAGE in the absence of reducing agent.

Photocrosslinking assays using unlabeled AET and radiolabeled oligonucleotide were performed as described above, except that ^{125}I-AET was replaced with 0.75 nMol of unlabeled dry AET dissolved in 10 μl of buffer A, and unlabeled oligonucleotide was replaced with an equivalent amount of ^{32}P-labeled oligonucleotide.

Thiol Occlusion Assay

Cy3-maleimide was synthesized according to a method described for Cy5-maleimide synthesis [23]. For the thiol occlusion assay, 60 μl of buffer A was preincubated at room temperature for 15 min with either VP39 alone (0.01 nMol), a mixture of VP39 and VP55 (0.01 nMol of each), or a mixture of VP39, VP55, and oligo UU-(dC)$_{25}$-U (0.01 nMol of each). To initiate reactions, mixtures were transferred to microcentrifuge tubes containing ~1 nMol of dry Cy3-maleimide. At various times, 10 μl samples were withdrawn and mixed with 3 μl aliquots of 4× SDS-PAGE sample buffer (0.25 M Tris-HCl [pH 6.8], 8% [w/v] SDS, 40% [v/v] glycerol, 0.04% bromphenol blue, 20% [v/v] 2-merchaptethanol) to stop the reactions. Samples were loaded on 13% SDS-PAGE gels. Wet gels were fluorimaged using a Molecular Imager FX (Bio-Rad), and relative amounts of protein-linked Cy3 were determined by quantitation of the resulting digital signals using Quantity One software (Bio-Rad).

Chemical Nuclease Assay

Conjugation of VP39 mutants with FeBABE and affinity cleavage of oligonucleotide were performed as described [24] with slight modifications. Briefly, 50 μl of 1 μM purified VP39 in 10 mM HEPES-NaOH (pH 8.0), 25 mM NaCl, 1 mM EDTA, 0.01% Nonidet P-40 (buffer B) was mixed with 2 μl of 26 mM FeBABE (stock solution in dimethylsulfoxide). After 4 hr at room temperature, excess FeBABE was removed by overnight dialysis against buffer B at 4°C. The degree of FeBABE conjugation was determined by transferring an aliquot to microcentrifuge tubes containing ~1 nMol of dry Cy3-maleimide and incubating at room temperature for 30 min, followed by SDS-PAGE as outlined above ("Thiol Occlusion Assay").

Five picomoles each of FeBABE-conjugated VP39, VP55, and ^{32}P end-labeled oligo UU-(dC)$_{25}$-U were mixed in 4 μl of buffer B and incubated at room temperature for 1 hr. Cleavage reactions were initiated by the addition of 0.5 μl of 50 mM ascorbate (free acid [pH 7.0]) and 0.5 μl of 5% (v/v) hydrogen peroxide, followed by incubation at room temperature for 15 min. Postcleavage samples were ethanol precipitated, redissolved in water, supplemented with an equal volume of formamide, and subjected to urea-PAGE (15% T, 5% C). After electrophoresis, gels were dried under vacuum and imaged using a PhoshorImager (Molecular Dynamics). Lines drawn through gel lanes were quantitated using ImageQuant software. The resulting data were transfered to a spreadsheet for alignment of data from the different lanes and data subtraction.

Acknowledgments

We thank Xiaoqun Duan and Dr. Florante A. Quiocho (HHMI, Baylor College of Medicine) for help with the molecular modeling program GRASP, Dr. Claude F. Meares for kindly providing the FeBABE reagent, and Dr. Richard Ebright for helpful discussions. This study was supported by National Institutes of Health grant R01 GM501953.

Received: January 11, 2001
Revised: March 21, 2002
Accepted: April 17, 2002

References

1. Schnierle, B.S., Gershon, P.D., and Moss, B. (1992). Cap-specific mRNA (nucleoside-O$^{2'}$-)-methyltransferase and poly(A) polymerase stimulatory activities of vaccinia virus are mediated by a single protein. Proc. Natl. Acad. Sci. USA *89*, 2897–2901.
2. Schnierle, B.S., Gershon, P.D., and Moss, B. (1994). Mutational analysis of a multifunctional protein, with mRNA 5′ cap-specific (nucleoside-2′-O-)-methyltransferase and 3′-adenylyltransferase stimulatory activities, encoded by vaccinia virus. J. Biol. Chem. *269*, 20700–20706.
3. Gershon, P.D., and Moss, B. (1993). Stimulation of poly(A) tail elongation by the VP39 subunit of the vaccinia virus-encoded poly(A) polymerase. J. Biol. Chem. *268*, 2203–2210.
4. Moss, B., Rosenblum, E.N., and Gershowitz, A. (1975). Characterization of a polyriboadenylate polymerase from vaccinia virions. J. Biol. Chem. *250*, 4722–4729.
5. Gershon, P.D., Ahn, B.-Y., Garfield, M., and Moss, B. (1991). Poly(A) polymerase and a dissociable polyadenylation stimulatory factor encoded by vaccinia virus. Cell *66*, 1269–1278.
6. Xiang, Y., Latner, D.R., Niles, E.G., and Condit, R.C. (2000). Transcription elongation activity of the vaccinia virus J3 protein in vivo is independent of poly(A) polymerase stimulation. Virology *269*, 356–369.
7. Hodel, A.E., Gershon, P.D., Shi, X., and Quiocho, F.A. (1996). The 1.85 Å structure of vaccinia protein VP39: A bifunctional enzyme that participates in the modification of both mRNA ends. Cell *85*, 247–256.
8. Hodel, A.E., Gershon, P.D., Shi, X., Wang, S.-M., and Quiocho, F.A. (1997). Specific protein recognition of an mRNA cap through its alkylated base. Nat. Struct. Biol. *4*, 350–354.
9. Hodel, A.E., Gershon, P.D., and Quiocho, F.A. (1998). Structural basis for sequence non-specific recognition of 5′-capped mRNA by a cap modifying enzyme. Mol. Cell *1*, 443–447.
10. Hodel, A.E., Quiocho, F.A., and Gershon, P.D. (1999). VP39 – an mRNA cap-specific 2′-*O*-methyltransferase. In Structure and Function of AdoMet-Dependent Methyltransferases, X. Cheng and R.M. Blumenthal, eds. (Singapore: World Scientific Publishing Co./Imperial College Press), pp. 255–282.
11. Shi, X., Yau, P., Jose, T., and Gershon, P.D. (1996). Methyltransferase-specific domains within VP39, a bifunctional protein which participates in the modification of both mRNA ends. RNA *2*, 88–101.
12. Shi, X., Bernhardt, T.G., Wang, S.-M., and Gershon, P.D. (1997). The surface region of the bifunctional vaccinia RNA modifying protein VP39 that interfaces with poly(A) polymerase is remote from the RNA binding cleft used for its mRNA 5′ cap methylation function. J. Biol. Chem. *272*, 23292–23302.

13. Deng, L., Johnson, L., Neveu, J.M., Hardin, S., Wang, S.M., Lane, W.S., and Gershon, P.D. (1999). A polyadenylylation-specific RNA-contact site on the surface of the bifunctional vaccinia virus RNA modifying protein VP39 that is distinct from the mRNA 5′ end-binding "cleft." J. Mol. Biol. *285*, 1417–1427.
14. Gershon, P.D., Shi, X., and Hodel, A.E. (1998). Evidence that the RNA methylation and poly(A) polymerase stimulatory activities of vaccinia virus protein VP39 do not impinge upon one another. Virology *246*, 253–265.
15. Johnson, L., and Gershon, P.D. (1999). RNA binding characteristics and overall topology of the vaccinia poly(A) polymerase-processivity factor complex. Nucleic Acids Res. *27*, 2708–2721.
16. Deng, L., Beigelman, L., Matulic-Adamic, J., Karpeisky, A., and Gershon, P.D. (1997). Specific recognition of an rU_2-N_{15}-rU motif by VP55, the vaccinia virus poly(A) polymerase catalytic subunit. J. Biol. Chem. *272*, 31542–31552.
17. Chen, Y., Ebright, Y.W., and Ebright, R.H. (1994). Identification of the target of a transcription activator protein by protein-protein photocrosslinking. Science *265*, 90–92.
18. Heilek, G.M., and Noller, H.F. (1996). Directed hydroxyl radical probing of the rRNA neighborhood of ribosomal protein S13 using tethered Fe(II). RNA *2*, 597–602.
19. Johnson, L., and Gershon, P.D. Positive readout of protein thiol-FeBABE derivatization. Biotechniques, in press.
20. Meisenheimer, K.M., and Koch, T.H. (1997). Photocross-linking of nucleic acids to associated proteins. Crit. Rev. Biochem. Mol. Biol. *32*, 101–140.
21. Deng, L., and Gershon, P.D. (1997). Interplay of two uridylate-specific RNA binding sites in the translocation of poly(A) polymerase from vaccinia virus. EMBO J. *16*, 1103–1113.
22. Thomson, J.G., and Gershon, P.D. (1995). Use of vaccinia virus poly(A) polymerase for RNA 3′-end labeling with either a chain-terminating nucleotide or a short 3′ homopolymer tract. Biotechniques *19*, 416–425.
23. Callaci, S., Heyduk, E., and Heyduk, T. (1998). Conformational changes of Escherichia coli RNA polymerase sigma70 factor induced by binding to the core enzyme. J. Biol. Chem. *273*, 32995–33001.
24. Owens, J.T., Miyake, R., Murakami, K., Chmura, A.J., Fujita, N., Ishihama, A., and Meares, C.F. (1998). Mapping the σ^{70} subunit contact sites on *Escherichia coli* RNA polymerase with a σ^{70}-conjugated chemical protease. Proc. Natl. Acad. Sci. USA *95*, 6021–6026.
25. Nicholls, A., Sharp, K.A., and Honig, B. (1991). Protein folding and association: insights from the interfacial and thermodynamic properties of hydrocarbons. Proteins *11*, 281–296.
26. Gershon, P.D., and Moss, B. (1996). Expression, purification, and characterization of vaccinia virus-encoded RNA and poly(A) polymerases. In Methods in Enzymology, L.C. Kuo, D.B. Olsen, and S.S. Carroll, eds. (Orlando, FL: Academic Press), pp. 208–227.
27. Sayle, R.A., and Milner-White, E.J. (1995). RASMOL: biomolecular graphics for all. Trends Biochem. Sci. *20*, 374.